U.S. DEPARTMENT OF THE INTERIOR
U.S. GEOLOGICAL SURVEY

Prepared in cooperation with the
CALIFORNIA DEPARTMENT OF TRANSPORTATION

SCIENTIFIC INVESTIGATIONS MAP 2852

INTRODUCTION

The 1982-83 and 1997-98 El Niños brought very high precipitation to California's central coast; this precipitation resulted in raised groundwater levels, coastal flooding, and destabilized slopes throughout the region. Large landslides in the coastal mountains of Big Sur in Monterey and San Luis Obispo Counties blocked sections of California State Route 1 (hereafter, Coast Highway 1), closing the road for months at a time. Large landslides such as these occur frequently in the winter months along the Big Sur coast due to the steep topography and weak bedrock. A large landslide in 1983 resulted in the closure of Highway 1 for over a year to repair the road and stabilize the slope. Resulting work from the 1983 landslide cost over $7 million and generated 30 million cubic yards of debris from landslide removal and excavations to re-establish the highway along the Big Sur coast (Engellenner, 1984).

Before establishment of the Monterey Bay National Marine Sanctuary (MBNMS) in 1992, typical road opening measures involved disposal of some landslide material and excess material generated from slope stabilization onto the seaward side of the highway. It is likely that some or most of this disposed material, either directly or indirectly through subsequent erosion, was eventually transported downslope into the ocean. In addition to the landslides that initiate above the road, natural slope failures sometimes occur on the steep slopes below the road and thus deliver material to the base of the coastal mountains where it is eroded and dispersed by waves and nearshore currents. Any coastal-slope landslide, generated through natural or anthropogenic processes, can result in sediment entering the nearshore zone. The waters offshore of the Big Sur coast are part of the MBNMS (fig. 1). Since it was established in 1992, landslide-disposal practices came under question for two reasons. The U.S. Code of Federal Regulations, Title 15, Section 922.132 prohibits discharging or depositing, from beyond the boundary of the Sanctuary, any material or other matter that subsequently enters the Sanctuary and injures a Sanctuary resource or quality. The landslide-disposal practices previously used had the potential to alter nearshore zone habitat by converting marine habitats from rocky substrate to soft bottom. In addition, the disposal practices had the potential to increase concentrations of suspended sediment in the nearshore zone, and thereby possibly impact coastal biological communities. On the other hand, natural mass-wasting processes, including coastal cliff erosion coastal and landslides, as well as streams deliver sediment to the coast in unknown quantities and thus provide nutrients as well as source material for beaches. Current road maintenance and repair practices along the Coast Highway 1 corridor that restrict disposal of material within the MBNMS may actually reduce sediment input relative to natural processes.

PURPOSE

The purpose of this study is to quantify the long-term volume of sediment entering the nearshore zone from coastal mass wasting, including landslides and cliff erosion, along the approximately 120-km-long Big Sur coast from south of the Carmel River to San Carpoforo Creek (fig. 1). The geographic limits of the study correspond to that part of the coast where the steep slopes of the Santa Lucia Range descend uninterrupted to the Pacific Ocean along the Big Sur coast. The primary goals of the research are to quantify the volume of sediment that enters MBNMS through coastal landslide processes using historical and recent aerial stereo photographs, to map the temporal and spatial variations in landslide distribution along the coast, and to relate the volume losses to the complex geology of the region to document the geologic controls on sediment yield from coastal landslides. The Coast Highway Management Plan (CHMP) was established with the intention of developing highway management approaches and solutions collaboratively with the MBNMS. This study is undertaken as a direct result of the need identified by Caltrans and MBNMS staff of a fundamental lack of data on background sediment volumes entering the MBNMS from coastal landslides.

STUDY AREA

The Big Sur coast lies on the west boundary of the Coast Ranges, a northwest-trending series of mountains and valleys flanking the coast from near Santa Barbara, California, to the Oregon border. In the Big Sur area, the Santa Lucia Range reaches elevations of nearly 1,600 m within 5 km of the coast, making it one of the steepest coastal slopes in the conterminous United States.

GEOLOGIC SETTING

The rocks along the Big Sur coast are a complex mixture of sheared and metamorphosed sedimentary and igneous rocks of the Late Jurassic to Miocene Franciscan Complex, and Mesozoic plutonic and metamorphic rocks of the Sur Complex of Hall (1991). Maps featuring these units and references to additional studies can be found in reports by Dibblee (1974), Ross (1976), and Hall (1991). The Franciscan Complex crops out along much of the California coast, and it records a period of time when the active plate boundary between the North American and Pacific Plates was convergent rather than the present day strike-slip. The rocks of the Franciscan Complex are probably the remains of an ancient accretionary wedge that formed when oceanic plate material and overlying oceanic sediments were scraped up as the Farallon Plate was subducted beneath the North American Plate (Blake and others, 1988). These rocks were subsequently transported northward along the San Andreas Fault to their present position. The predominant Franciscan Complex rock types exposed along the Big Sur coast include metavolcanic rocks (greenstone), serpentinite, and interbedded, highly sheared argillite and graywacke (Bailey and others, 1964). The 108 to76-Ma plutonic rocks of the Sur Complex of hall (1991) (James and Mattinson, 1988) form the core of the Salinian block, which is bound on the east side by the San Andreas Fault, and on the west by the Sur-Nacimiento Fault. The granitic and metamorphic rocks of the Salinian block represent a part of the ancestral Sierra Nevada range that has been transported along the San Andreas Fault to its present position in central California (Page, 1982). The Sur Complex of Hall (1991) rocks exposed along the Big Sur coast (table 1; fig. 2) are quartz diorite and charnockitic tonalite, respectively (Compton, 1966; Ross, 1976). The study area was divided into nine sections, as shown on figure 2 and described in table 1, on the basis of those individual stretches of coast along which the aerial photography could successfully be orthorectified, and terrain data derived for the analysis. These nine study sections are within both Franciscan Complex and Sur Complex of Hall (1991) rocks (table 1; fig. 2). The Salinian and Franciscan bedrock is overlain in many areas by a relatively thick blanket of debris composed of poorly bedded silts, sands, and beds of angular cobbles and boulders; much of the original bedrock geology is also disrupted by numerous landslide deposits (Hall, 1991; Wills and others, 2001).

The rocks of the Franciscan Complex tend to be weaker than those of the Sur Complex of Hall (1991); the majority of the recurring landslides occur where Franciscan Complex rocks underlie the steep slopes. However, the lithology within the Franciscan Complex varies dramatically, and the softer, highly sheared rocks and mélange are more prone to landsliding whereas the various sedimentary strata and volcanic rocks form more stable slopes.

CLIMATE AND WAVES

The Big Sur region, like much of the central California coast, experiences a Mediterranean (temperate) climate; this climate is marked by most precipitation falling in the winter months and mild temperatures throughout the year. The weather in the region is predominantly controlled by the North Pacific High: its presence during the summer produces dry westerly winds and upwelling of fog-producing, cold ocean water, and its absence in the winter results in high rainfall concentrated in a period between October and May (Gilliam, 1962). Rainfall amounts vary with elevation. Lower slopes near the coast may receive less than half the rainfall that falls near the top of the mountains. The average annual rainfall near the town of Big Sur from 1914 to 1987 was 109 cm; it is estimated that approximately 230 cm falls higher on the slopes (Henson and Usner, 1993).

Much of the Big Sur coast is directly exposed to Pacific storms. Waves reach the base of the coastal slope along the entire coastline except where a few larger pocket beaches have formed. The continental shelf along much of the Big Sur coast is considerably narrower than the shelf to the north or south. The shelf width ranges from approximately 12 km at Point Sur to less than 5 km for most of the Big Sur coastline (California Coastal Commission, 1987). The shelf is steeper along the Big Sur coast and as a result, there may be less dissipation of deep-water wave energy as waves travel across the shelf (Komar, 1998), and if this assumption is true, waves meet the shoreline with higher energy than where the shelf is wider and more gently sloping.

For most of the year, swells along this part of the coast are from the northwest. Data from the National Oceanic and Atmospheric Administration National Data Buoy Center show average significant wave heights at Cape San Martin (see fig. 3*C*) of 9 m in the winter months of January and February. Wave periods in the winter average 18 s. The mean tide range along the Big Sur coast is 1.3 m, with a diurnal range of 1.7 m (California Coastal Commission, 1987).

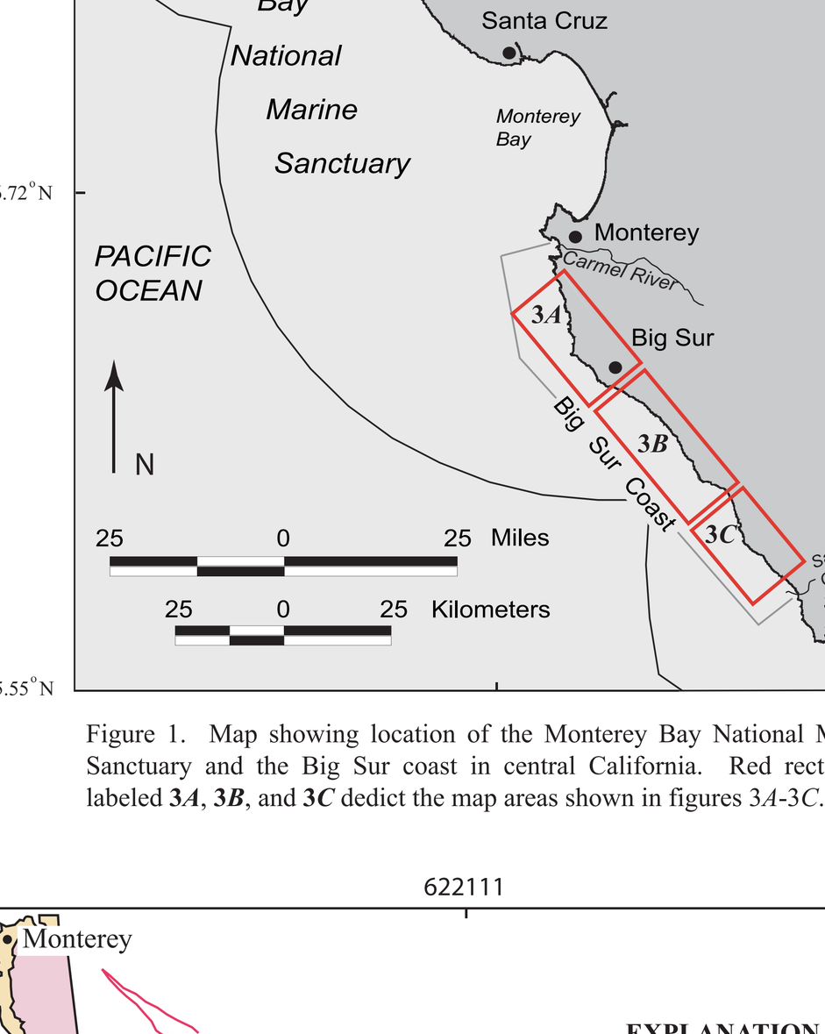

Figure 1. Map showing location of the Monterey Bay National Marine Sanctuary and the Big Sur coast in central California. Red rectangles labeled **3*A***, **3*B***, and **3*C*** dedict the map areas shown in figures 3*A*-3*C*.

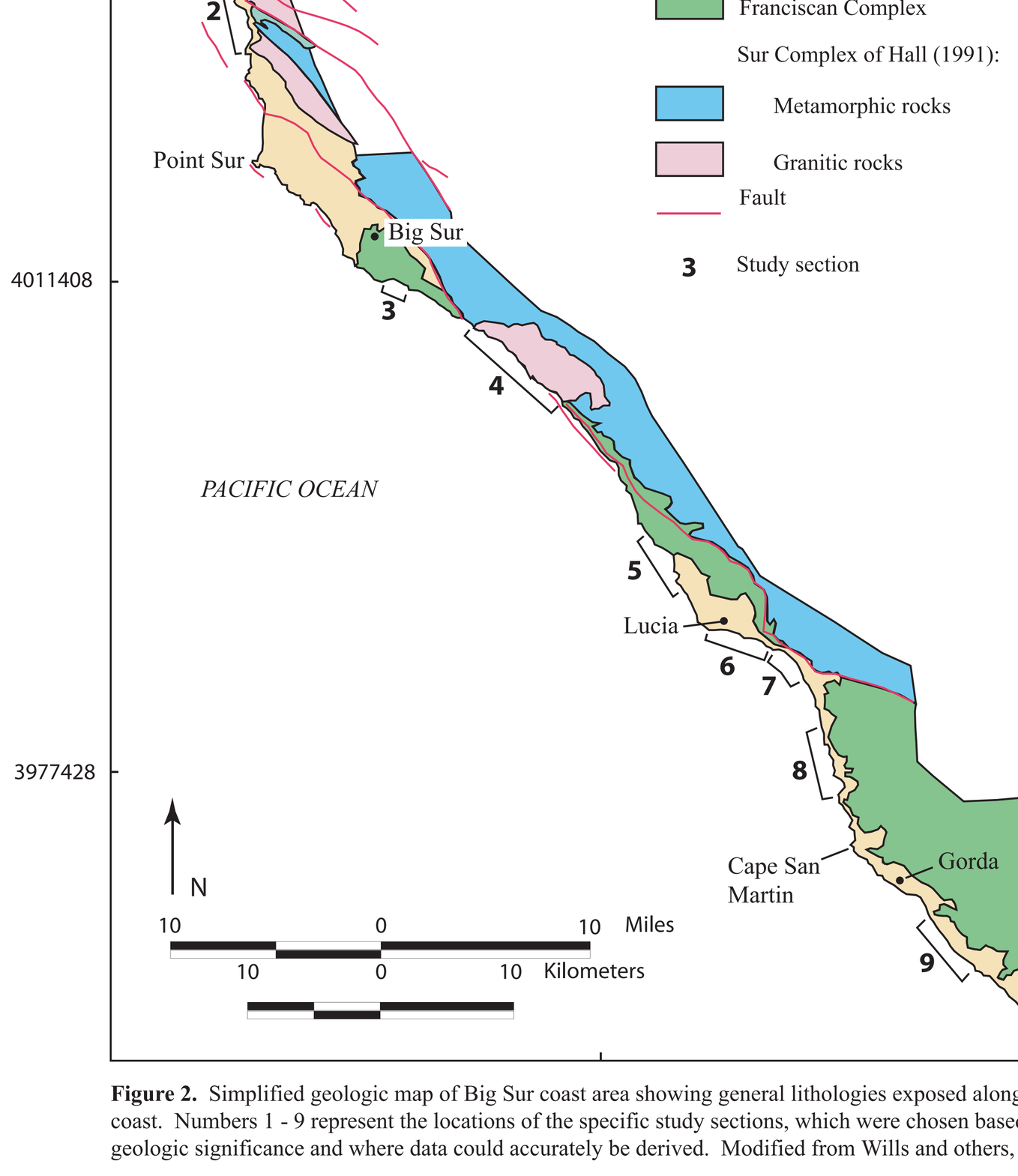

Figure 2. Simplified geologic map of Big Sur coast area showing general lithologies exposed along the coast. Numbers 1 - 9 represent the locations of the specific study sections, which were chosen based on geologic significance and where data could accurately be derived. Modified from Wills and others, 2001.

Table 1. Geologic units found in each of the nine study sections near Big Sur, California (from mapping by Wills and others, 2001).

Study section No.	Post Mile*	Primary (I) and secondary (II) geologic unit	Description**
1	63.1-66.0	I. Kqd I. Qdf	Cretaceous hornblende-biotite quartz diorite--medium to dark gray coarse-grained. Debris-fan deposits; nearly continuous and overlapping.
2	59.5-63.0	I. Kqd I. KMct II. Qdf	Cretaceous hornblende-biotite quartz diorite. Charnockitic tonalite--dark greenish gray, coarse-grained; very fractured and sheared. Debris fan deposits; nearly continuous and overlapping.
3	45.6-46.6	I. KJf II. Qls	Undifferentiated Franciscan Complex. Landslide deposits; discontinuous.
4	36.8-41.5	I. KMct II. Qls	Charnockitic tonalite. Landslide deposits; discontinuous.
5	26.0-29.2	I. KJfmv I. KJf II. Qls	Franciscan Complex metavolcanics. Franciscan Complex mélange. Landslide deposits; continuous and overlapping.
6	21.3-24.1	I. KJfmv II. Qls	Franciscan Complex metavolcanic rocks--fine-grained, hard, metamorphosed basalt; occur as blocks in mélange or landslide deposits. Landslide deposits; continuous and overlapping.
7	19.4-21.2	I. KJfgw I. KJfs II. Qls	Franciscan Complex metavolcanic rocks. Franciscan Complex mélange. Landslide deposits; continuous and overlapping.
8	14.0-17.4	I. KJfmv I. KJfgw I. KJfs II. Qdf/Qom/Qls	Franciscan Complex metavolcanic rocks. Franciscan Complex graywacke--fine-grained to medium-grained sandstone; occurs interbedded with highly sheared argillite. Franciscan Complex Serpentinite--gray to green highly sheared and foliated. Debris-fan deposits, continuous/ marine-terrace deposits/ landslide deposits; discontinuous.
9	73.0(SLO) 3.5 (MON)	I. KJfgw I. KJfs II. Qls	Franciscan Complex graywacke. Franciscan Complex Serpentinite. Landslide deposits; continuous and overlapping.

*Post miles are for Monterey County (MON) unless otherwise noted; SLO, San Luis Obispo County.
**A rock type is described only the first time it is listed in the table.

METHODS

The primary tools used in this study are digital photogrammetry and geographic information system (GIS). Digital photogrammetry involves the processing of historical and recent vertical aerial photographs to produce Digital Terrain Models (DTMs) from 3-D stereo models. These time-sequence DTMs are brought into a GIS where volume changes are calculated, and then the spatial distribution of the terrain changes can be analyzed and compared to the local geology. The historical aerial photographs chosen for this study are from 1942 (1:30,000), and the recent photographs are from 1994 (1:24,000). These photographs provide the basis for determining a 52-year, end-point volumetric change for the nine study sections shown on figures 3*A*-3*C*. These particular groups of aerial photographs were chosen because their scales provided regional coverage of the coastline, the length of time between them provided the longest possible time period for the long-term rate calculation, and their availability as stereo film positives (diapositives) minimized nonsystematic errors.

DIGITAL PHOTOGRAMMETRY

Digital photogrammetry requires a specific workflow that results in the production of orthophotographs (digital images from which all displacements have been removed) and DTMs. To create true orthophotographs, displacements inherent in unrectified photography must be corrected to make accurate measurements from the images. The displacements include those related to the camera system, the camera position, and the terrain relief (Slama, 1980; Falkner, 1995; Wolf and Dewitt, 2000). Interior orientation adjusts the images according to the camera system by incorporating known calibrated information from the camera, such as the focal length, radial lens distortion, and distance between fiducial points. Exterior orientation corrects for changes in the position of the sensor platform through a series of points that tie a strip of images to one another in image space and uses ground-control point data along with aerotriangulation to perform a best-fit mathematical transformation for assigning geographic coordinates to the images.

Once the interior and exterior orientations have been applied, the resulting images are partially rectified. However, accurate measurements cannot be made until the effects of relief displacement are removed, which is especially crucial in a high-relief terrain such as that along the Big Sur coast. Removal of relief displacement requires the creation and incorporation of a DTM. The DTMs in this study were built from the stereo images using a Triangulated Irregular Network (TIN) of elevation points rather than a standard grid model to best capture the steep and rapidly changing topography (Hapke and Richmond, 2000; Maune and others, 2001). TINs and grids are simply different ways of storing and representing data in a DTM or a DEM (digital elevation model), respectively.

Prior to photogrammetric processing, the original film diapositives acquired for this study were converted to digital format by scanning at high resolution (approximately 1,200 dpi) with a photogrammetric scanner. The images were then imported into commercial photogrammetry software to perform all corrections and to create and edit the TIN while viewing in stereo. Stereo-viewing capabilities ensure the accurate placement of breaklines and allow the removal or adjustment of erroneous data points, including those on buildings, on vegetation, and in water.

For digital photogrammetric processing that requires high accuracy, ground-control points for orthorectification are usually photo-identifiable points that are surveyed in the field using a differential global positioning system (DGPS). Because it was necessary during this study to produce DTMs of large stretches of remote coastline, ground surveying was impractical for collection of ground-control points. In lieu of ground-survey data, ground-control points for the recent (1994) aerial photography were derived from U.S. Geological Survey digital orthophotoquadrangles (DOQs) for horizontal control, and 30-m National Elevation Data that were adjusted using supplemental ground-survey data to improve vertical resolution for vertical control. The errors associated with these control data were incorporated into the overall model error analysis outlined in the section called "Error Analysis."

Obtaining ground-control data for historical photography, especially in a relatively undeveloped and remote area such as the Big Sur region, presents additional challenges in the creation of orthophotographs and DTMs. For this study, the recent (1994) images were rectified and a DTM was created prior to the processing of the historical (1942) images. The recent images and resulting DTMs were then used to derive the control for the 1942 images. In many cases the extrapolated control includes features such as individual rocks in outcrops that appear to be stable in the period between photographs, as well as features associated with road intersections, driveways, and parking lots. Thus, the historical model is rectified relative to the recent model; this improves the overall accuracy by allowing for a sufficient number and distribution of ground control points. Because the objective of the study was to determine the change from one period to the next, the relative change between the two surface models accurately represents the differences.

A final step prior to exporting the orthophotographs and the DTMs from the photogrammetry software was to determine the areas for each section under which the sediment volumes were calculated. This step was completed within the photogrammetry software so that the 3-D viewing capabilities of the software can be used to digitize polygons that accurately represent natural breaks in the terrain. Because this study was designed to determine the volumetric input to the nearshore directly from coastal landslides, the polygons do not include any major drainages that extend upland beyond the first ridge crest. Furthermore, the polygon perimeters outline topographic breaks that define the direct coastal slope, or the slope along which material in transport would most likely travel directly to the base of the slope and not into an adjacent drainage. Because the determination of the polygons involves distinguishing topographic breaks, stereo-viewing capabilities were essential.

GEOGRAPHIC INFORMATION SYSTEM (GIS)

Once the topographic surface models are generated and edited, they are exported from the photogrammetry software and into a GIS. The orthophotomosaics and delineated polygons generated for each study section are also brought into a GIS, and all layers including other existing data sets such as geologic maps and field data maps can be viewed and analyzed using geographic coordinates. GIS provides a number of tools that can be used to conduct detailed terrain analyses, including volume calculations, slope analyses, and contouring of various data sets.

The volume for each topographic surface model is calculated from the two dates, above a datum of 1.0 m above mean sea level. The 1.0 m represents the lowest elevation from which photogrammetric stereo models can be confidently viewed without significant visual interference from the movement of waves on the water and on the lower part of the beach (Hapke and Richmond, 2000). The volumes from the two dates of photography are then subtracted and averaged over the polygon areas along each section of coast. This averaging smooths out the noise generated by localized volume gains in areas where movement on a specific slide has deposited material. Finally, the average value is divided by the total time between the photographs (52 years). This provides an average volumetric loss rate for each section of coast along the length of each polygon.

In addition to the rate change determination, orthophotographs and georeferenced images were used in conjunction with the polygons of volumetric change to map locations and spatial distribution of historically active landslides. To supplement the 1942 and 1994 analysis of landslide distribution, 1929 aerial photographs were obtained for the study area. Although they are not of sufficient quality to create stereo models, they were georeferenced using the 1994 orthophotographs for control. The distribution of active slopes was then digitized for three dates: pre-highway (1929), immediately post-highway (1942), and recent (1994). The active slopes were visually identified as areas of bare earth (not vegetated).

ERROR ANALYSIS

Four primary sources of error were identified for the volume change and sediment yield estimates in this study. The errors include those associated with 1) the accuracy of the control points, 2) the accuracy of block models, 3) the vertical accuracy of the DTM, and 4) the accuracy of the images based on the pixel resolution. Control-point errors are related to the accuracy of the original data source for the control. For the 1994 imagery, x and y positional errors of 7 m are associated with the U.S. Geological Survey DOQs from which the ground-control points were identified Accuracy standards for the original DEM data allow for vertical errors of approximately 7-12 m. However, the subsequent adjustment of the DEM using surveyed features, such as roads, within the coverage area resulted in a model with an accuracy on the order of 1 m, based on point comparisons of the DEM with lidar data that became available after the processing was completed. For the 1942 models, the control-point data were derived from the corresponding 1994 models. The control-point accuracy for the 1942 models is the total computed uncertainty associated with the 1994 models (E_t) and ranges from 9.2 to 11.0 m.

The source of the rectification error (e_r) for both dates of imagery is the standard deviation of the control-point error within each block from the photogrammetric processing (Slama, 1980; Wolf and Dewitt, 2000). For this study the value propagated through the uncertainty analysis is two standard deviations, which provides a 95% confidence level. This assumes that the errors are nonsystematic (random) and are normally distributed. The rectification error varies from model to model, and it is highly dependent on the amount, distribution, and quality of the ground control used in the rectification process.

The vertical accuracy of the DTM (e_d) is a function of the scale of the photographs, and hence the flying height and camera focal length, from which the DTMs are created. The DTM accuracy is estimated as 1/9000th of the flying height of the aircraft carrying the camera system (Maune, 2001). In this study, the flying height of the 1994 photographs was 4,000 m and the flying height of the 1942 photographs was 5,000 m resulting in vertical errors of 0.4 m and 0.5 m, respectively. In addition, Saleh (2001) recommends applying an environmental factor (EF), ranging from one to five, to compensate for nonsystematic errors in the model. Such nonsystematic errors that could affect the vertical accuracy of the DTM include extreme relief, linear distribution of ground control, distortion of original film (shrinkage and stretching), lack of camera calibration information, and high radial distortion within the photographs. For the models developed during this study, an environmental factor of two was applied to the recent (1994) data on the basis of extreme relief and linear distribution of ground control. An environmental factor of five was applied to the historical (1942) data because all of the nonsystematic errors affected the data. While the EF has not been rigorously tested, it provides a means of maximizing the DTM error when the environmental conditions are less than ideal. The DTM error (e_d) component of the total error analysis is 0.72 m for the 1994 DTM, and it is 2.3 m for the 1942 DTM.

Finally, the pixel resolution of the scanned photographs is included in the error analysis; it represents the visual limitation of identifying an object (or location) that is smaller in dimension than the pixel size of the digital image. The pixel size of the 1994 images is 0.5 m and for the 1942 images it is 0.7 m.

The total error associated with the model for each date is determined by

$$E_t = [(e_g)^2+(e_r)^2 + (e_d)^2 + (e_p)^2]^{0.5}$$

where e_g is control-point error, e_r is 2 times the standard deviation of the rectification error, e_d is DTM error, e_p is pixel resolution; and the subscript t is a given time, or date, from which the data are derived.

The total model error is translated to an uncertainty in sediment volume (δ_{vt}) by averaging the calculated error over the area within which the volume was calculated by

$$\delta_{vt} = (E_t * A)/Vt$$

where *A* is the area over which the volume was calculated (table 2) and *Vt* is the volume calculated for a particular date. This equation produces a percent volume of the total estimated volume that is within the uncertainty range for that dataset. To determine the total uncertainty in the volume change calculation, the uncertainties for the two dates are summed

$$Total\ error = \delta_{v1994} + \delta_{v1942}$$

The total uncertainty for the volumes and sediment yields generated for this study range from a low of 9.8% to a high of 24.4% (table 2).

SEDIMENT YIELD FROM COASTAL LANDSLIDES

The results of the volumetric change analysis are shown in table 2. The area covered by each section, the shore-parallel length, the total volume loss and the losses per linear extent of coast (sediment yield) are provided for nine study sections of coast along with descriptions of the geologic units from Wills and others (2001). The average estimated sediment yield for the Coast Highway 1 corridor is approximately 21,000 ± 3,200 m^3 /km/yr on the basis of the analysis for the nine study sections. Sections 1 and 2, shown in Figure 3*A*, have very low input rates for the coastline compared to other sections (table 2). Both Sections 1 and 2 lay within the stronger granitic material. Sections 6 and 7, shown in Figure 3*B* have moderately high input rates for the coastline compared to other sections (table 2). Section 4 lies within the stronger granitic material, and it has anomalously high input rates compared to the surrounding areas (study sections 3 and 5). This high rate is attributed to the large landslide that occurred in 1983 and is, therefore, within the 52-year time period of this analysis. Stabilization of this landslide was the largest earth-moving operation in the Big Sur region; a total of nearly 20 million cubic meters of material was removed by both natural processes and slope stabilization. Sections 8 and 9, shown in the map of the southern section (fig. 3*C*), have the highest input rates for the coastline compared to other sections (table 2). The rocks along this section of coastline are faulted and sheared rocks of the Franciscan Complex and this section of the coast has a history of large, well-known landslides (Wills and others, 2001).

Owing to unresolvable nonsystematic errors associated with the 1942 photographs, accurate 3-D models could not be created for the entire coast. These errors most likely result from distortions in the original film (stretching and warping of old film) as well as radial distortion associated with older mapping cameras that becomes especially prevalent in areas of extreme relief, such as along much of the Big Sur coast. Because the sediment yield for the entire coastline cannot be determined using the DTM differencing method described herein, the sediment yield is interpolated in areas of missing data by correlating the bedrock lithology and landslide density of areas without measured data to areas where the sediment yield was determined. Results of the sediment yield analysis from DTM differencing show a strong correlation between the local geology and the sediment delivery rates (fig. 4). The interpolation assumes sediment volumes will be similar (within an order of magnitude) in areas with similar underlying bedrock and density of historical landslides.

The sediment yield data vary significantly and range from 1,000 ± 240 m^3/km/yr in study section 1 (fig. 3*A*) to a high of 46,700 ± 7,300 m^3/km/yr in study section 8, north of the town of Gorda (fig. 3*C*). The variation in the delivery rate of sediment to the base of the slope appears to be closely related to the primary lithology within a given area (fig. 4). In general, the lowest sediment yield is from the granitic rocks of the Sur Complex of Hall (1991) and the resistant sandstone of the Franciscan Complex, and the highest yield is in the highly sheared mélange of the Franciscan Complex.

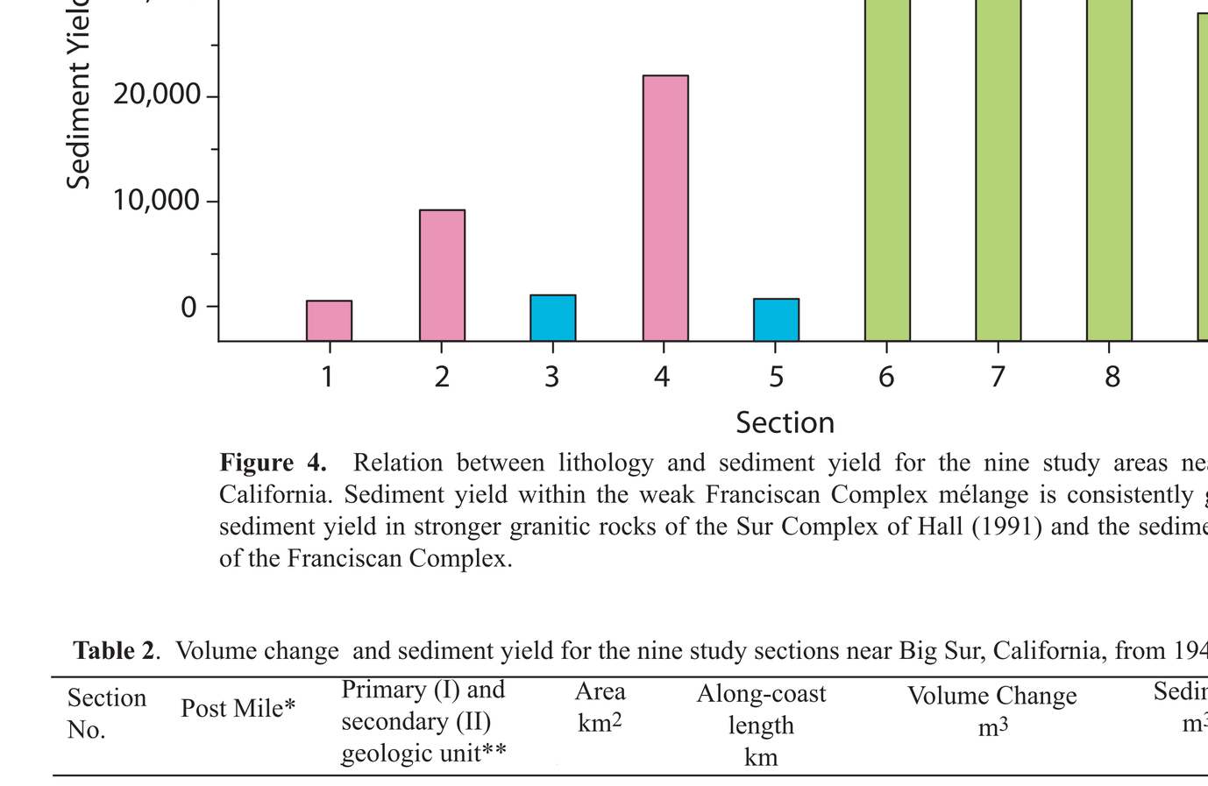

Figure 4. Relation between lithology and sediment yield for the nine study areas near Big Sur, California. Sediment yield within the weak Franciscan Complex mélange is consistently greater than sediment yield in stronger granitic rocks of the Sur Complex of Hall (1991) and the sedimentary rocks of the Franciscan Complex.

Table 2. Volume change and sediment yield for the nine study sections near Big Sur, California, from 1942-1994.

Section No.	Post Mile*	Primary (I) and secondary (II) geologic unit**	Area km^2	Along-coast length km	Volume Change m^3	Sediment yield m^3/km/yr
1	63.1-66.0	I. Kqd I. Qdf	2.3	4.5	234,000 ± 57,100	1,000 ± 240
2	59.5-63.0	I. Kqd, KMct II. Qdf	3.1	5.5	2,750,000 ±671,000	9,600 ± 2,300
3	45.6-46.6	I. KJf II. Qls	1.3	2.5	158,000 ± 5,500	1,200 ± 120
4	36.8-41.5	I. KMct II. Qls	5.0	7.3	8,328,000 ± 999,400	21,900 ± 2,600
5	26.0-29.2	I. KJfmv, KJf II. Qls	3.2	5.3	313,000 ± 48,800	1,100 ± 170
6	21.3-24.1	I. KJfmv II. Qls	3.5	5.0	11,700,000 ± 1,954,000	45,100 ± 7,000
7	19.4-21.2	I. KJfmv, KJfs II. Qls	1.2	3.0	4,936,000 ± 770,000	31,600 ± 4,900
8	14.0-17.4	I. KJfmv, KJfgw, KJfs II. Qdf/Qom/Qls	4.7	8.0	19,400,000 ± 3,026,000	46,700 ± 7,300
9	73.0(SLO)-3.5	I. KJfgw, KJfs II. Qls	3.0	5.0	7,100,000 ± 745,500	27,700 ± 3,000

*All post miles are in Monterey County unless otherwise noted; SLO, San Luis Obispo County.
**Refer to table 1 for descriptions of geologic units.

ACTIVE SLOPE DISTRIBUTION

Digital orthophotoquadrangles from 1994 and georeferenced imagery of the Big Sur coast from 1942 and 1929 were used to map the distribution of active slopes for each date. Active slopes were identified by areas showing evidence of recent disturbance, such as complete lack of vegetation and clear landslide scars (for example, headscarps). These areas correspond in part to the historical landslides mapped by Wills and others (2001). However, individual active slope delineations do not necessarily define the entire extent of a particular landslide, rather only that portion of a landslide or cliff face that was active at the time the photographs were taken. The linear distribution of active slopes for each year is shown on figure 3 as strips parallel to the coastline. Each of the three active slope strips represents the coast-parallel extent of areas where subaerial active slopes were identified for a particular date of aerial photography.

From the temporal and spatial distribution of landslides, it is evident that much of this region was undergoing active slope failure during the construction of Coast Highway 1 in 1929, and in many places the slopes were again active in both 1942 and 1994. The most active area for all time periods for the entire Big Sur coast are the study sections shown on figure 3 that correspond well to the weaker rocks of the Franciscan Complex. The rocks within these sections are predominantly highly sheared mélange of the Franciscan Complex and are substantially weaker than the granitic rocks of the Sur Complex of Hall (1991) and the less sheared rocks of the Franciscan Complex to the north.

SUMMARY

Coast Highway 1 in Monterey and San Luis Obispo Counties extends along the rugged and remote Big Sur coast at the base of the Santa Lucia Range. The region is tectonically active and continued uplift has created one of the steepest coastal slopes in the contiguous United States. The steep slopes are, along much of this coast, formed in the very weak mélange of the Franciscan Complex. In addition, this region experiences both high amounts of precipitation and high wave energy in the winter months. All these factors combine to produce an area of chronic landslides that regularly block, undermine, or damage this road. Large volumes of material often must be removed from the highway after a landslide, and additional material is frequently generated when the slopes are stabilized to prevent further damage to the highway. The water extending from the base of the slopes along the entire Big Sur coast is part of the MBNMS and it is against federal regulations to dump or dispose of any material into a national marine sanctuary owing to the possibility of negatively impacting the nearshore habitat.

The purpose of this study is to provide background information on the volumes of sediment and other material that historically enter the MBNMS along the Big Sur coast directly from coastal landslides and to map both the spatial and temporal distribution of areas of active input. Using digital stereo photogrammetry, terrain models were created for two dates spanning a 52-year time period. The volume change was then calculated by differencing the terrain models. A sediment yield (volume loss per linear extent of coast per year) was derived using this method for nine sections of coastline. The average sediment yield was 21,000 ± 3,200 m^3/km/yr, with a range of 1,000 ± 240 m^3/km/yr in section 1 (fig. 3*A*) to a high of 46,700 ± 7,300 m^3/km/yr in section 8 (fig. 3*C*). The largest sediment yields are within the weakest materials that are concentrated in the southern part of the study area, while the lowest sediment yields were within the stronger rocks, located primarily in the northern part of the Big Sur coast. In the areas where the sediment yield could not be directly calculated, the yields were interpolated by correlating with the geology in areas where sediment yields were determined. The interpolated areas are shown as dashed lines on figure 3.

In addition to the sediment yield data for the coast, figures 3*A*-3*C* also show the distribution of active slopes along the coast. Using georeferenced photography from 1929 (which pre-dates the construction of the road) along with the photography from 1942 and 1994 used in the volumetric analysis, locations of active slopes were digitized in a GIS.

Figures 3A-3C show that both the locations of the active slopes, as identified in the three dates of photographs, and the higher sediment yields are associated with the weak rocks of the Franciscan Complex. These areas of Franciscan Complex rocks also correspond to areas of historical and dormant landslides mapped by Wills and others (2001). This pattern suggests that the locations and rates of material influx to the nearshore zone is not a recent phenomenon--rather it has been occurring for hundreds or even thousands of years. The technique of estimating the sediment yield from the coastal landslides provides the necessary background data to determine the average volumetric sediment input along the coast.

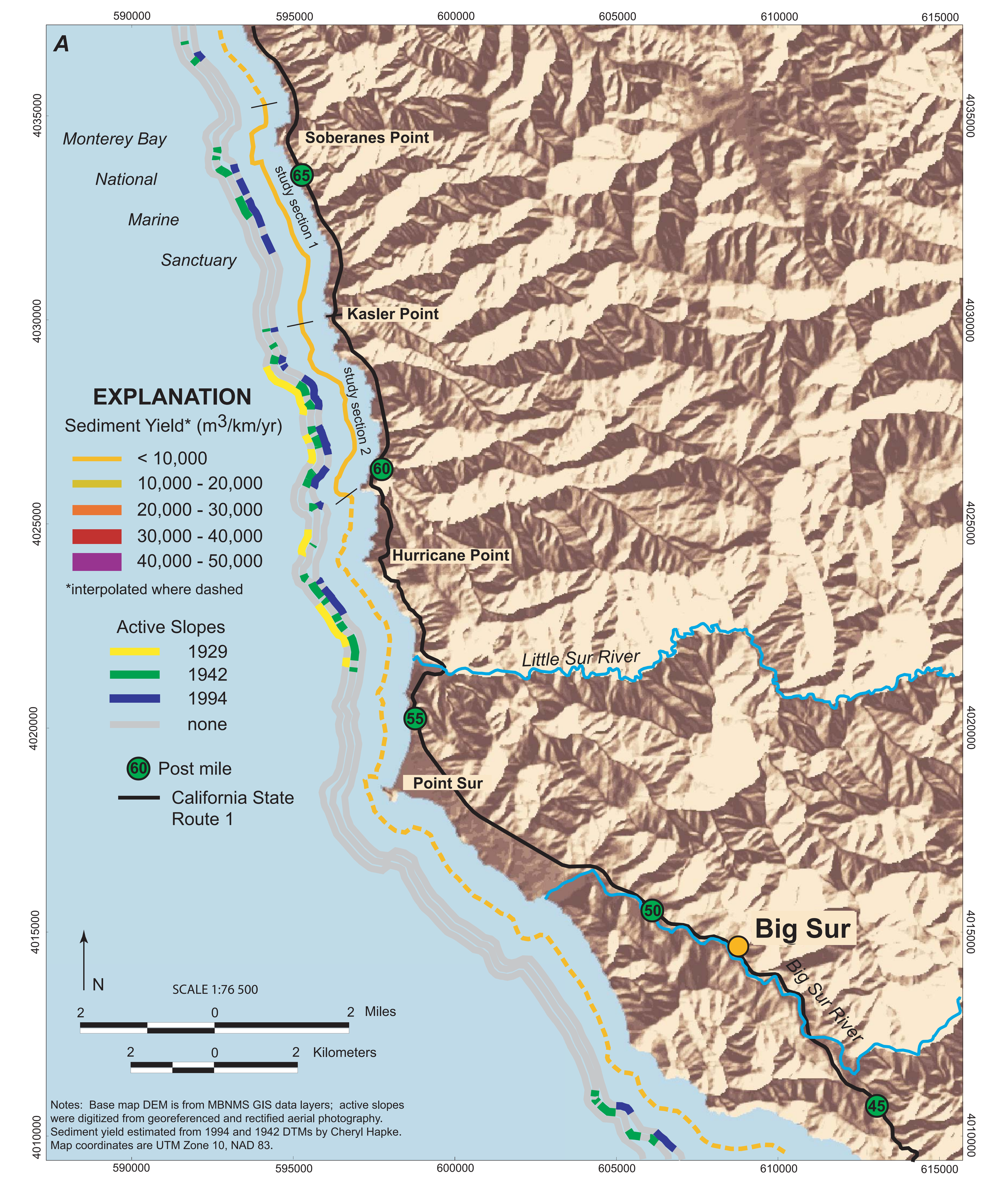

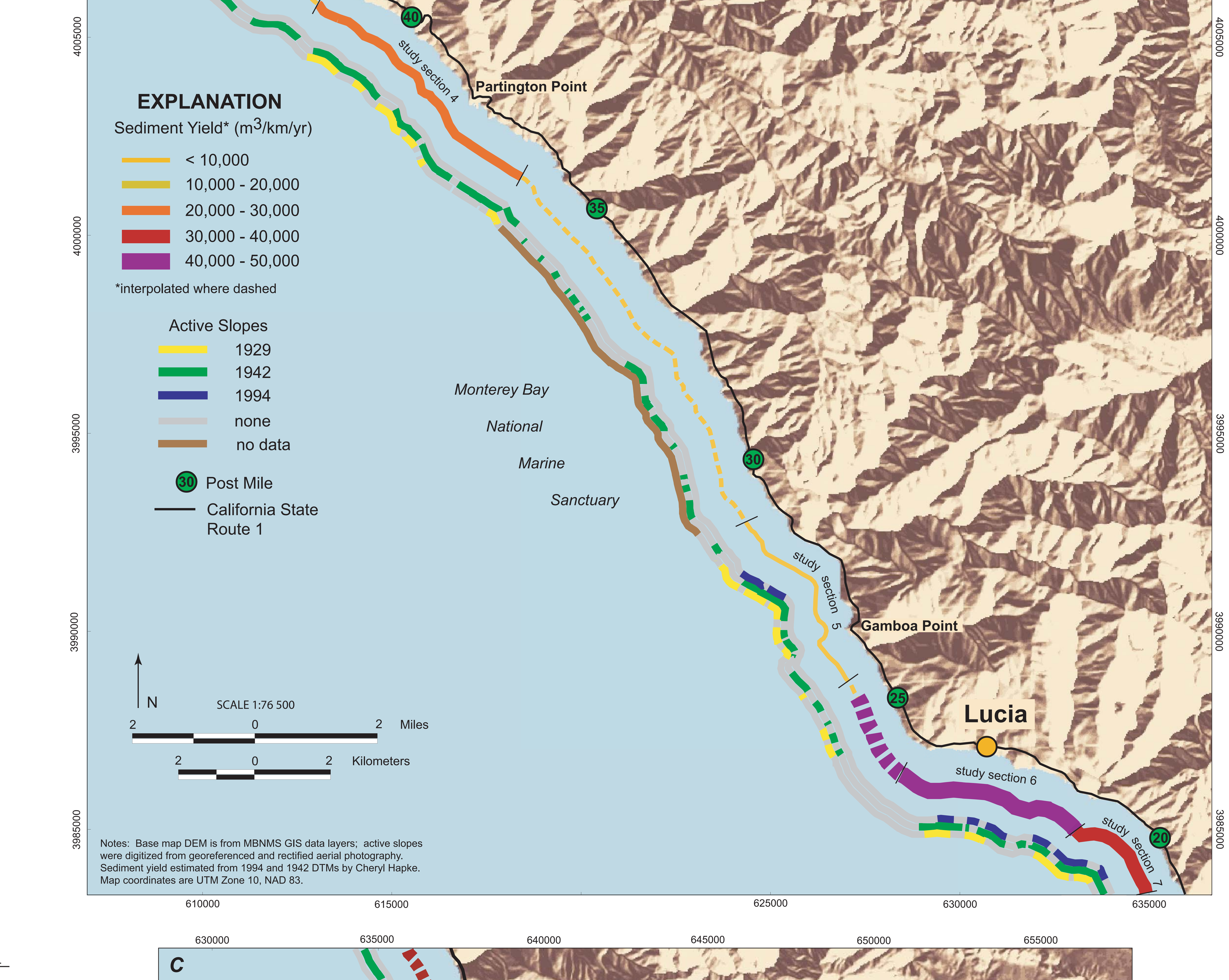

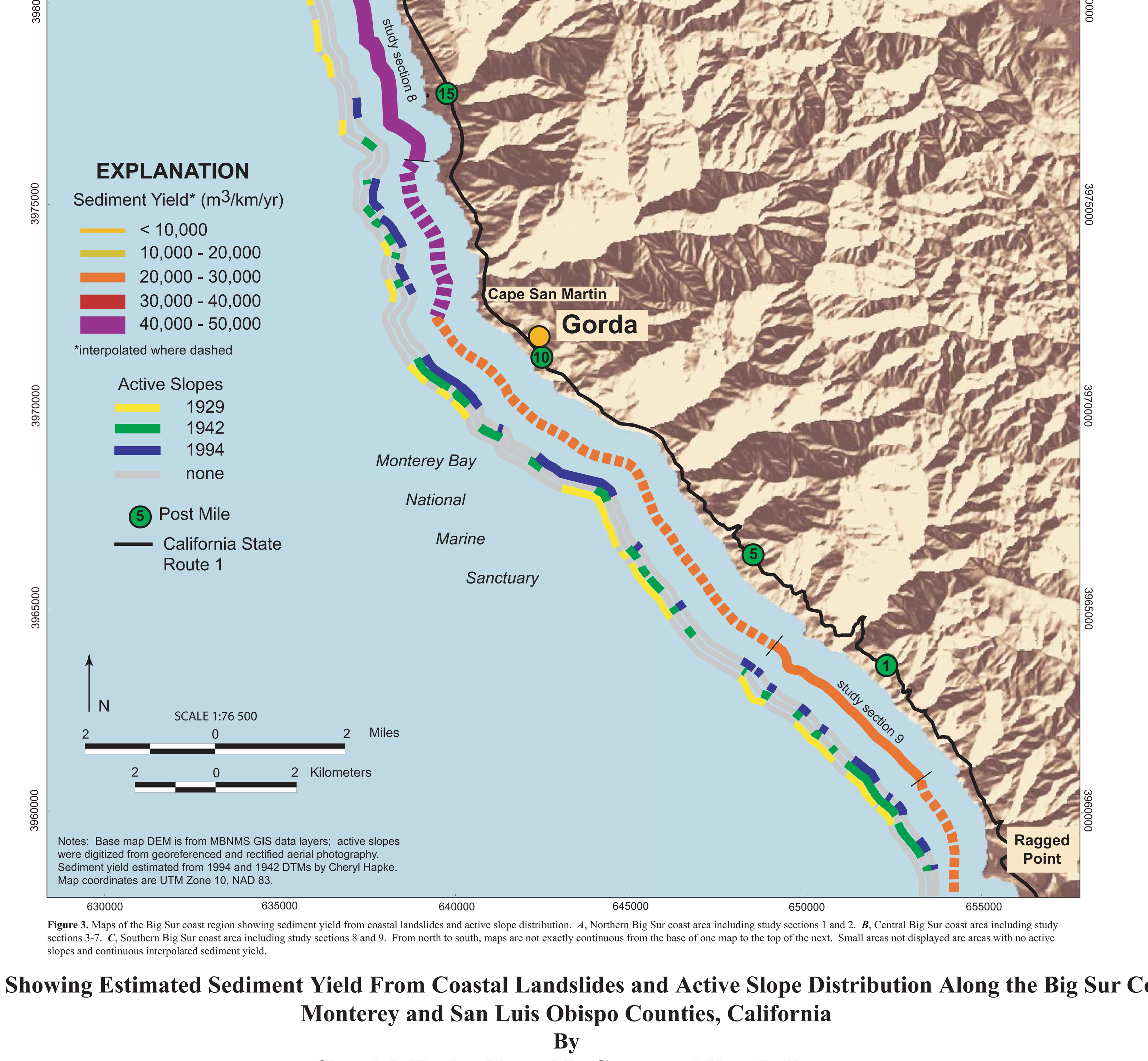

Figure 3. Maps of the Big Sur coast region showing sediment yield from coastal landslides and active slope distribution. ***A***, Northern Big Sur coast area including study sections 1 and 2. ***B***, Central Big Sur coast area including study sections 3-7. ***C***, Southern Big Sur coast area including study sections 8 and 9. From north to south, maps are not exactly continuous from the base of one map to the top of the next. Small areas not displayed are areas with no active slopes and continuous interpolated sediment yield.

REFERENCES

Ackerman, F., 1996, Techniques and strategies for DEM generation, in Greve, C.W., ed., Digital Photogrammetry--An addendum to the manual of photogrammetry: Bethesda, Md., American Society for Photogrammetry and Remote Sensing, p. 135-141.
Bailey, E.H., Irwin, W.P., and Jones, D.L., 1964, Franciscan and related rocks and their significance in the geology of western California: California Division of Mines and Geology Bulletin 183, 177 p.
Blake, M.C., Jr., Jayko, A.S., McLaughlin, R.J., and Underwood, M.B., 1988, Metamorhpism and tectonic evolution of the Franciscan Complex, northern California, in Ernst, W.G., ed., Metamorphism and crustal evolution of the western United States, Rubey Volume 7: Englewood Cliffs, New Jersey, Prentice-Hall, p. 1035-1060.
California Coastal Commission, 1987, California Coastal Resource Guide: Berkeley, University of California Press, 384 p.
Compton, R.R., 1966, Granitic and metamorphic rocks of the Salinian block, California Coast Ranges: California Division of Mines and Geology Bulletin 190, p. 277-287.
Dibblee, T.W., Jr. 1974, Geologic maps of the Monterey, Salinas, Gonzales, Point Sur, Jamesburg, Soledad, and Junipero Serra quadrangles, Monterey County, California: U.S. Geological Survey Open-File Report 74-1021, 1 sheet, scale 1:62,500.
Engellenner, J., 1984, Party reopens scenic highway: The Sentinel (Santa Cruz, Ca), April 12, 1984.
Falkner, E., 1995, Aerial Mapping Methods and Applications: Boca Raton, Fla., Lewis Publishers, 322 p.
Gilliam, H., 1962, Weather of the San Francisco Bay region, Natural History Guide 6: Berkeley, University of California Press, 72 p.
Hall, C.A., Jr., 1991, Geology of the Point Sur-Lopez Point region, Coast Ranges, California--a part of the Southern California allochthon: Geological Society of America Special Paper 266, 40 p.
Hapke, C.J. and Richmond, B.M., 2000, Monitoring beach morphology changes using small-format aerial photography and digital softcopy photogrammetry: Environmental Geosciences, v. 7, no. 1, p. 32-37.
Henson, P., and Usner, D.J., 1993, The natural history of Big Sur: Berkeley, University of California Press, 416 p.
James, E.W., and Mattinson, J.M., 1988, Metamorphic history of the Salinian block--an isotopic reconnaissance, in Ernst, W.G., ed., Metamorphism and crustal evolution of the western United States, Rubey Volume 7, Englewood Cliffs, New Jersey, Prentice-Hall, p. 938-952.
Komar, P.D., 1998, Beach processes and sedimentation: Upper Saddle River, New Jersey, Prentice Hall, 544 p.
Maune, D.F., Kopp, S.M., Crawford, C.A., and Zervas, C.E., 2001, Introduction--digital elevation models, in Maune, D.F., ed., Digital elevation model technologies and applications -- The DEM users manual: Bethesda, Maryland, American Society of Photogrammetry and Remote Sensing, p. 1-34.
Page, B.M., 1982, Migration of Salinian composite block, California, and disappearance of fragments: American Journal of Science, v. 282, p. 1694-1734.
Ross, D.C., 1976, Reconnaissance geologic map of the pre-Cenozoic basement rocks, northern Santa Lucia Range, Monterey County, California: U.S. Geological Survey Miscellaneous Field Studies Map MF-750, 1 sheet, 1:125,000.
Saleh, R.A., 2001, A handle on the accuracy of imagery-based digital elevation data in a softcopy environment, Workshop #2, Measuring the Earth-Digital Elevation Technologies and Applications: MAPPS-ASPRS Conference, Oct. 29 – Nov. 2, 2001, St. Petersburg, Fla., 45 p.
Slama, C., ed., 1980, Manual of Photogrammetry: Falls Church, Virg., American Society of Photogrammetry, 1056 p.
Wills, C.J., Manson, M.W., Brown, K.D., Davenport, C.W., and Domrose, C.J., 2001, Landslides in the Highway 1 Corridor: Geology and Slope Stability Along the Big Sur Coast, Report to the Coast Highway Management Plan Caltrans District 5, 29 p.
Wolf, P.R., and Dewitt, B.A., 2000, Elements of photogrammetry with applications in GIS (3rd ed.): Boston, McGraw Hill, 608 p.

Maps Showing Estimated Sediment Yield From Coastal Landslides and Active Slope Distribution Along the Big Sur Coast, Monterey and San Luis Obispo Counties, California

By
Cheryl J. Hapke, Krystal R. Green, and Kate Dallas
2004

125 years of science for America 1879–2004

Manuscript approved for publication August 25, 2004

This map was printed on an electronic plotter from digital files. Dimensional calibration may vary between electronic plotters and between X and Y directions on the same plotter, and paper may change size due to atmospheric conditions; therefore, scale and proportions may not be true on plots of this map.

For sale by U.S. Geological Survey, Information Services, Box 25286, Federal Center, Denver, CO 80225, 1-888-ASK-USGS

Available on the World Wide Web at http://pubs.usgs.gov/sim/2004/2852